

Gas phase sorting of nanoparticles

Hendrik Ulbricht, Martin Berninger, Sarayut Deachapunya, André Stefanov and Markus Arndt
Quantum Optics, Quantum Nanophysics and Quantum Information,
Faculty of Physics, University of Vienna, Boltzmannngasse 5, A - 1090 Vienna, Austria
 (Dated: November 8, 2018)

We discuss Stark deflectometry of micro-modulated molecular beams for the enrichment of biomolecular isomers as well as single-wall carbon nanotubes and we demonstrate the working principle of this idea with fullerenes. The sorting is based on the species-dependent polarizability-to-mass ratio α/m . The device is compatible with a high molecular throughput, and the spatial micro-modulation of the beam permits to obtain a fine spatial resolution and a high sorting sensitivity.

Sorting of nanoparticles is essential for many future nanotechnologies. Nanoparticles can generally be sorted by their different physical or chemical properties. The objective is to prepare or enrich a particular species with a distinct property. In the case of carbon nanotubes the sorting of species with different metallicity is essential for many applications such as the realization of field effect transistors, light emitting diodes or conducting wires [1]. Here sorting can for instance be achieved by exploiting the tube's dielectric properties in a liquid environment [2]. Also chemical methods for the selection and separation of carbon nanotubes are currently being investigated [3].

Complementary to these efforts also the manipulation of large clusters and molecules in the gas phase has attracted a growing interest over recent years, in particular with applications in molecule metrology [4, 5, 6, 7]. Since many nanoparticles, among them biomolecules or carbon nanotubes, exist in various different isomers and conformations, it is intriguing to investigate sorting methods in the gas phase which select the particles according to their polarizability-to-mass ratio α/m instead of their mass alone.

A large number of classical deflection experiments have been performed in the past (for a review see [6]) which employ the deflection of a well-collimated neutral beam in the presence of a static transverse inhomogeneous electric field. In this arrangement, one can usually choose between a wide molecular ray of high flux or a narrow beam with a lower total signal whose lateral shift can be determined with higher precision.

We here present a method for sorting nanoparticle beams which combines high transmission *and* high resolution. This can be achieved by imprinting a very fine spatial modulation onto the molecular beam.

Our starting point is a three-grating matter-wave interferometer which we already described before [8]. As shown in Fig. 1, it is composed of three micro-machined gratings, which prepare, sort and detect the molecules. The combination of the first two gratings modulates the particle flux such as to generate a periodic particle density pattern in the plane of the third grating. All gratings and also the molecular micro-modulation have identical periods. The density pattern or contrast function can therefore be revealed by scanning the third grating while

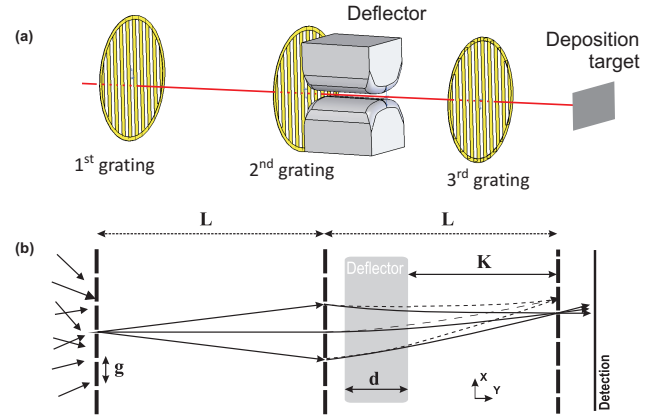


FIG. 1: (a) Three grating deflection setup. The third grating can be shifted to scan the nanoparticle fringe pattern. Particles with different α/m are separated by their different deflection shifts in the electrode field as identified in (b). The grating position can be set to preferentially transmit one species while blocking the others. After the sorting the molecules may be deposited on a target or detected by ionization.

counting all transmitted molecules, as shown in Fig. 2.

Our device is usually operated in a quantum mode, with molecular masses and velocities chosen such as to reveal fundamental quantum phenomena related to matter-wave diffraction [9].

However, the same device can also be used in a Moiré or shadow mode [10], where the molecules can be approximated by classical particles. This applies in particular to fast and very massive molecules where quantum wave effects may be too small to be observed.

Our setup then still combines a fine spatial micro-modulation with much relaxed requirements on the collimation of the beam. This allows us to increase the spatial resolution in any beam-displacement measurements by several orders of magnitude over earlier experiments without micro-imprint.

A beam-displacement may for instance be caused by an inhomogeneous electric field acting on the polarizability of the particle. In our experiment of Fig. 1, a pair of electrodes close to the second grating generates a constant force field $F_x = \alpha(\mathbf{E}\nabla)E_x$, which shifts the molecular

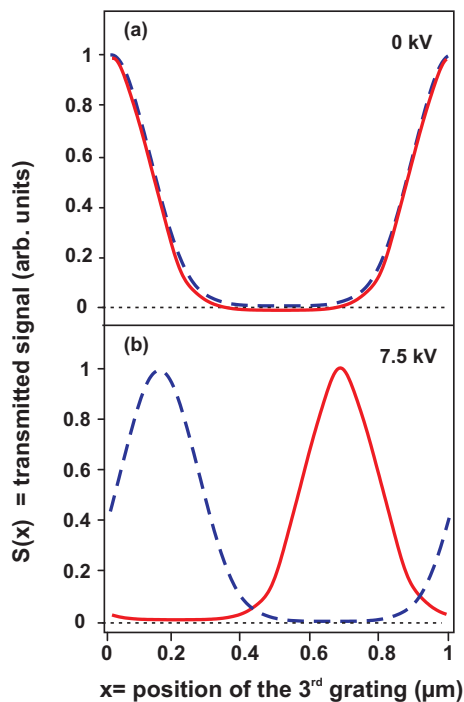


FIG. 2: Predicted fringe pattern for YGW and YWG tripeptides. (a) shows the calculated density distribution after the third grating without applying any voltage to the deflecting electrodes: The full curve is the YWG and -- belongs to the YGW peptide. (b) indicates that already at 7.5 kV both biomolecules can be separated and therefore maximally enriched. The calculation takes also into account the dispersive interaction of the molecules with the metal gratings. The transmission function is periodic in x with over many thousand lines, with a grating constant of 990 nm in this example.

fringe pattern along the x -axis by

$$\Delta s_x \propto (\alpha/m) \cdot (\mathbf{E}\nabla)E_x/v_y^2. \quad (1)$$

Here v_y is the beam velocity in the forward direction. Deflection measurements then allow to derive precise values for the polarizability of the molecules, as recently demonstrated [5, 7].

Here we extend the operation of our deflectometer to the classical Moiré mode with biomolecules and carbon nanotubes and we extend the previous molecular measurement to an active sorting method for molecular species that differ in α/m .

For a first illustration we discuss and simulate the relative enrichment of a 50:50 mixture of the tripeptide Tryptophan-Glycin-Tyrosin (YGW) and its isomer YWG which differ only by the swapped position of Glycin and Tryptophan in the amino acid sequence. Their masses are equal ($m=460$ u) but their susceptibilities $\chi(\text{YWG}) = 100 \text{ \AA}^3$ and $\chi(\text{YGW}) = 480 \text{ \AA}^3$ differ by almost a factor of five [11]. The susceptibility [12] $\chi = \alpha + \langle \mu_z^2 \rangle / (k_B T)$, includes the orientation averaged square of the projection of the electric dipole moment onto the direction of

the external field $\langle \mu_z^2 \rangle$ and T is the molecule temperature. With this definition, the polarizability in Eq. 1 may be replaced by χ , if the molecules also possess a permanent electric dipole moment.

For the two isomers the molecular fringe shifts will then differ by a factor of five, if all other beam parameters are equal. Therefore, when the three gratings are designed for maximum fringe contrast in the molecular beam close to the third grating, we may choose the electric field such that one sort of peptide will be transmitted by the deflectometer while its isomer will be blocked and deposited on the third grating. The transmitted beam will then reveal a significant enrichment of one particular isomer.

To quantify the sorting process we define the maximal enrichment of two mixed species P_1 and P_2 as:

$$\eta = \max_x \{ \tilde{S}_{P_1}(x) - \tilde{S}_{P_2}(x) \}, \quad (2)$$

where $\tilde{S}_{P_i}(x) = S(x)/[S_{max}(x) + S_{min}(x)]$ is the normalized signal of the Moiré curve associated with the peptide P_i (see Fig. 2), and x is the position of the third grating.

This definition is based on the fact that each isomer will form a fringe pattern with its own intensity, fringe visibility and beam shift in the external field gradient. Since the enrichment is meant to include only the effects of the sorting machine, the signals of both species are normalized to their average beam fluxes.

The definition is chosen such that $\eta = 0$ for equal normalized transmission of both species through the three-grating-arrangement, and $\eta = 1$ if one species is blocked while the other is fully transmitted.

For small polypeptides, the combination of a pulsed beam source with a pulsed laser detection scheme, may allow us to select a mean velocity of $v_y = 340$ m/s with a relative spread of $\Delta v_y/v_y = 0.5\%$. We now assume a grating separation of $L = 38.5$ cm, a grating constant of 990 nm, and a grating open fraction of $f = 0.2$, i.e. gap openings of 200 nm. Inserting all these parameters we find a relative enrichment for YWG as high as $\eta = 0.97$. The high expected degree of separation can also be seen in Fig 2b. Here, the voltage has been optimized to $(\mathbf{E}\nabla)E_x = 1.05 \times 10^{13} \text{ V}^2/\text{m}^3$ in order to maximize the transmitted content of this isomer. The required field can be generated between two convex 5 cm long electrodes at a difference potential of $U=7.5$ kV, and for a minimum distance of 4 mm.

Next to the sorting of biomolecules. The selection of carbon nanotubes with a defined internal structure is a challenge that has attracted great interest [1]. Our deflectometer proposal differs from earlier methods [2, 3] in that it is vacuum compatible and therefore better suited for a certain class of technological applications. It also differs from a recently patented suggestion for sorting free nanotube beams by laser fields [13] in that the use of microfabricated gratings allows us to combine an uncollimated molecular beam with a method of high spatial resolution.

In the following we will assume that it is in principle possible – even though technically difficult at present –

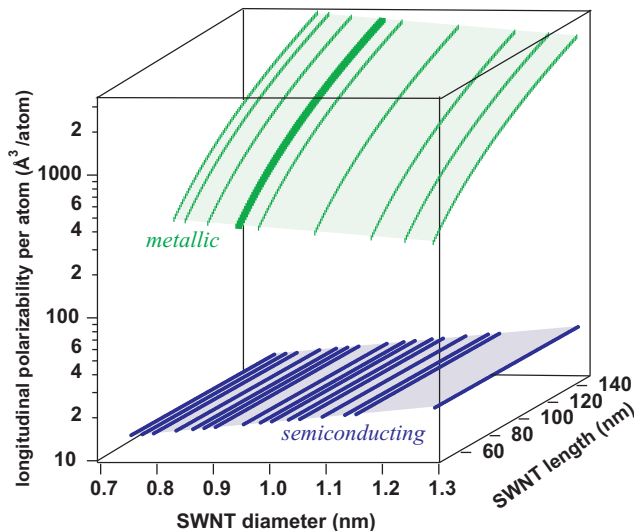


FIG. 3: Reduced longitudinal polarizability α_{\parallel} SWCNTs versus length and diameter. The two surfaces represent α_{\parallel} 's of metallic and semiconducting nanotubes of a typical diameter [14] and possible length distribution [15].

to generate a free molecular beam of single-wall carbon nanotubes (SWCNTs) with an assumed length distribution between 50 nm and 150 nm, an arbitrary mixture of chiralities and diameters between 0.7-1.3 nm.

To simulate the Moiré fringes for these nanotubes we first need to determine their α/m ratio. Their mass can be computed from the number of carbon atoms per unit cell [1]. The static polarizability of nanotubes is extremely anisotropic and we have to consider separately both the transverse and the longitudinal value per carbon atom, i.e. the reduced polarizabilities. The reduced transverse static polarizability of a carbon nanotube is independent of its metallicity but it is proportional to its radius R . For SWCNTs it can be approximated by $\alpha_{\perp red} \sim 1.3 \text{Å}^3/\text{atom}$ [17], a value very similar to that of C_{60} or medium-sized alkali clusters [18].

The longitudinal polarizability of semiconducting tubes $\alpha_{\parallel s}$ depends on their band gap energy E_g [17] according to $\alpha_{\parallel s} \propto (R/E_g^2)$. We use $\alpha_{\parallel s} \approx 8.2R^2 + 20.5$ for $R \geq 0.35$ nm [19]. Even for semiconducting SWCNTs the reduced longitudinal polarizability thus exceeds already the transverse value by about a factor of ten and the polarizability of medium-sized metal clusters by about a factor of two [20].

This relation for $\alpha_{\parallel s}$ can't be applied to metallic tubes because of their vanishing band gap, $E_g = 0$. We therefore approximate short metallic tubes of length l by perfectly conducting hollow cylinders [21] and find for their axial polarizability

$$\alpha_{\parallel m} = \frac{l^3}{24(\ln(l/R) - 1)} \left(1 + \frac{4/3 - \ln(2)}{\ln(l/R) - 1} \right). \quad (3)$$

This value exceeds that of equally long semiconducting tubes by a factor between ten and one hundred. In Fig. 3

we plot the reduced polarizabilities for a range of different tube diameters and lengths. The clear separation between metallic and semiconducting tubes in this diagram indicates that mixtures of these species will be well separable in a Moiré-deflection experiment.

The *reduced* longitudinal polarizability of semiconducting tubes does not scale with the tube's length, since both their mass and their polarizability grow linearly with it. The separation process will therefore also work for nanotubes beyond the parameter range of Fig. 3 [2].

With all masses and polarizabilities at hand, we now proceed to simulate the Moiré fringe patterns.

In Fig. 4 we show the simulations for two 100 nm long semiconducting (17,0) and metallic (9,0) nanotubes flying at 100 m/s with a velocity spread of $\Delta v_y/v_y = 1\%$ through a setup with metallic gratings separated by $L=38.5$ cm. The grating period is now set to $g = 10 \mu\text{m}$ and the open fraction is again $f=0.2$, which would permit a fringe contrast of 100% - for small classical balls without polarizability.

The semiconducting tube is computed to have $R=0.67$ nm, $m=3.2 \times 10^{-22}$ kg, $\alpha_{\perp} = 2.6 \times 10^4 \text{Å}^3$ and $\alpha_{\parallel} = 3.8 \times 10^5 \text{Å}^3$. The metallic tube has $R=0.36$ nm, $m=1.7 \times 10^{-22}$ kg, $\alpha_{\perp} = 9.5 \times 10^3 \text{Å}^3$ and $\alpha_{\parallel} = 1.1 \times 10^7 \text{Å}^3$. In the beginning we assume that all nanotubes are maximally aligned with respect to the external electric force field, i.e. along the x-axis. At a deflection field of $(\mathbf{E}\nabla)E_x = 1.4 \times 10^{12} \text{V}^2/\text{m}^3$, the metallic tube's fringe shift of 5200 nm would largely surpass the 150 nm shift of the semiconducting molecules. And one can easily find a voltage that will enrich the metallic tubes in the beam by shifting their fringe maxima until they fall onto the openings of the third grating, while the semiconducting tubes will be blocked by the grating bars. In this idealized picture the enrichment could reach almost 100% (Fig. 4A).

We now extend this simple model to include the attractive Casimir-Polder (CP) potential between the aligned molecules and ideally conducting grating walls in the approximation of long distances r :

$$U(r) = -\frac{3\hbar c}{8\pi} \frac{\alpha}{r^4}, \quad (4)$$

[22]. The influence of the CP interaction is demonstrated in Fig. 4 (b). The fringe contrast is reduced due to the deflection of the tubes in the grating's potential. For this simulation metal gratings are assumed and a larger enrichment can be maintained if the metal gratings are replaced by dielectric materials or even by gratings made of light [23, 24].

We also have to consider that any nanotube beam in the foreseeable future will carry molecules in a highly excited rotational state. Each orientation of the nanotube with respect to the external electrode field is associated with a different fringe shift, since the relative contributions by the transversal and longitudinal polarizability depend on this orientation.

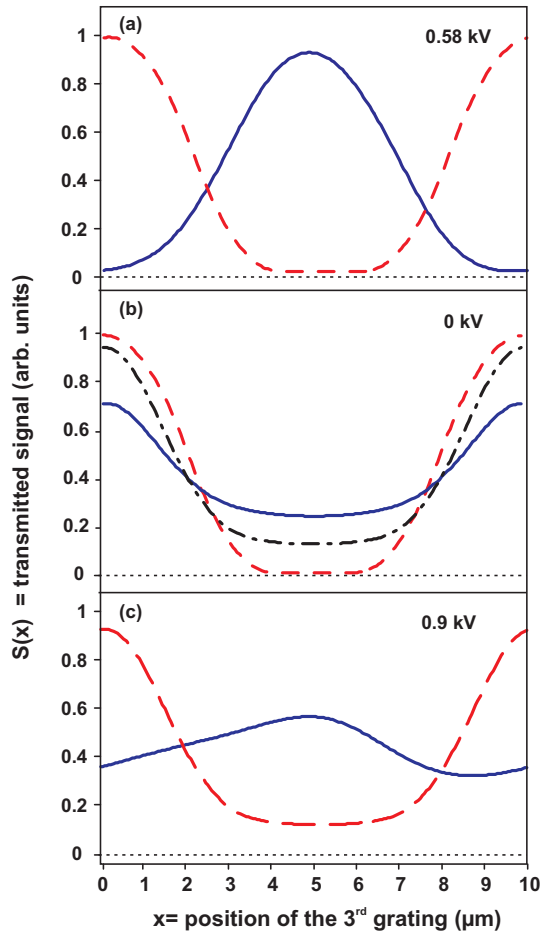


FIG. 4: Predicted fringe pattern for semiconducting (17,0) and metallic (9,0) carbon nanotubes. (a) illustrates the ideal Moiré case: The full curve is the (17,0) and $--$ belongs to the (9,0) tube without Casimir-Polder (CP) and maximal aligned at 0.58 kV. (b) shows the influence of the dispersive interaction between material grating and nanotube: $--$ is the Moiré pattern. $- \cdot -$ includes the CP interaction for the (17,0) and the full curve for the (9,0) tube at 0 kV [6] with maximum alignment, i.e. without rotation. (c) is the complete analysis including CP and full rotational averaging: The full curve is the (9,0) and $--$ is the (17,0) tube at 0.9 kV.

Fig. 4(c) shows an average of all Moiré curves now including both the full rotational distribution function [6] and the CP interaction. The expected fringe visibility still amounts to 77% for the semiconducting (17,0) tubes and to 31% for the metallic (9,0) ones. As can be seen from Fig. 4(c) this will allow a significant enrichment of the metallic tubes. The predicted value for the enrichment reaches $\eta(17,0) = 0.4$ for the semiconducting tubes and $\eta(9,0) = 0.6$ for the metallic ones. It is interesting to see that our reasoning still holds generally for all other chiralities. Metallic and semiconducting tubes will always be separable with a good probability, because of the huge variation in polarizabilities.

To demonstrate the working principle of our three-grating sorting machine we have performed experiments

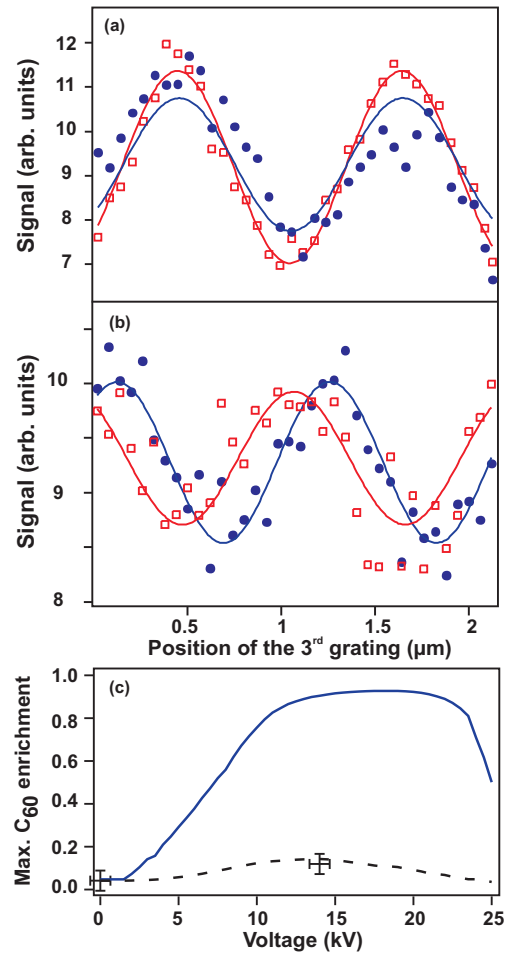


FIG. 5: A) Interference pattern without any voltage to the electrodes. B) Separation of C_{60} (circles) and C_{70} (squares) at an electrode voltage of 14 kV. The phase shift difference is $\delta = 171$ nm. Interference contrasts are normalized to the same height. C) Comparison between expected (dotted line) and observed maximal C_{60} enrichment at 0 kV and 14 kV in the existing setup (crosses) with $f=0.46$ and $\Delta v/v = 15\%$. The potential for larger fullerene enrichment with an optimized interferometer with $g=990$ nm, $f=0.2$ and $\Delta v/v = 1\%$ is indicated by the solid line.

with the fullerenes C_{60} and C_{70} in an existing Talbot-Lau interferometer with three identical gold gratings with a period of $g = 990$ nm and an open fraction of $f=0.46$. We detect the content of the different molecular species using a quadrupole mass spectrometer (QMS Extrel, 2,000 u). The two fullerenes C_{60} and C_{70} differ in their mass by the factor 7/6.

Their polarizability ratio was measured in a related experiment to be $\alpha_{C_{70}}/\alpha_{C_{60}} = 1.22$ [5]. The velocities in this mixture were 191 m/s for C_{60} and 184 m/s for C_{70} , both with a velocity spread of 15% from a thermal source. Fig. 5(a) shows the fringe contrast of the two fullerenes without any voltage applied to the electrodes. Even at $U = 0$ kV we already observe a slight enrichment due to the different fringe visibilities for C_{60} and C_{70} .

Applying a voltage of 14 kV then results in the phase-shift difference shown in Fig. 5 (b). Fig. 5 (c) plots the measured and expected enrichments of C_{60} , which are in rather good agreement.

The observed phase shift ratio $\Delta s(C_{70})/\Delta s(C_{60}) = 1.14$ fits well with our theoretical estimate (Eq. 1) of 1.13, including the statistical and systematic error of 4% in our experiment. For our experiment in Fig. 5 (b) we find a rather moderate C_{60} enrichment of $\eta(C_{60}) = 0.08$. This is obviously not yet optimized and it is interesting to discuss the factors that influence it in the present and in future experiments.

Secondly, the fringe contrast is very sensitive to the van der Waals interaction between the molecules and the grating walls. This attractive potential modulates the fringe visibility and it does this differently for different polarizabilities and molecule velocities. This influence can be reduced by choosing a wider grating period or by recurring to optical phase gratings, as mentioned before [8].

Thirdly, the Stark deflection itself is dispersive (Eq. 1). A finite velocity spread leads to a reduction of the interference contrast with increasing electric field. And while the fringes in our present experiment would tend to wash out beyond a deflection voltage of $U=14$ kV, pulsed beams of biomolecules [16] with $\Delta v_y/v_y \sim 0.1...1\%$ would be essentially free of such a restriction.

Fourthly, the polarizability ratio is rather small for the two fullerene species. In contrast to that, α/m may vary by $\sim 500\%$ for isomers of small polypeptides [11] and by even a factor up to one hundred for carbon nanotubes of

different chirality [17]. In this respect all future experiments will be simpler compared to our present demonstration.

The very good quantitative agreement between our experiment and the model expectations, shown in Fig. 5 (c) proves that we do understand the relevant processes in the present study. The solid line in Fig. 5 (c) shows the expected C_{60} enrichment in an interferometer setup which is optimized for sorting instead of quantum demonstrations.

Concluding, we have shown that α/m -variations can be used to sort neutral nanoparticles even in wide molecular beams. Our simulations show that the relative enrichment may even get close to 100% for biomolecular isomers and it will still be significant ($\sim 60\%$) for single-wall carbon nanotubes. The working principle is illustrated by the enrichment of C_{60} out of a mixed molecular beam composed of C_{60} and C_{70} fullerenes. The sorting scheme works in general for nanoparticles which can be transferred into a free molecular beam and which differ in their α/m ratio.

Acknowledgments

This work has been supported by the Austrian Science Funds (FWF) within the projects START177 and SFB F1505. We acknowledge fruitful discussions with Klaus Hornberger. S. D. acknowledges financial support by a Royal Thai government scholarship.

-
- [1] M. S. Dresselhaus, G. Dresselhaus, and P. Avouris, *Carbon Nanotubes. Synthesis, Structure, Properties and Applications* (Springer, Berlin, 2001).
- [2] R. Krupke, F. Hennrich, H. v. Löhneysen, and M. M. Kappes, *Science* **301**, 344 (2003).
- [3] M. S. Arnold, A. A. Green, J. F. Hulfat, S. I. Stupp, and M. S. Hersam, *Nature Nanotechnology* **1**, 60 (2006).
- [4] I. Compagnon, F. C. Hagemeister, R. Antoine, D. Rayane, M. Broyer, P. Dugourd, R. R. Hudgins, and M. F. Jarrold, *J. Am. Chem. Soc.* **123**, 8440 (2001).
- [5] M. Berninger, A. Stefanov, S. Deachapunya, and M. Arndt, *Phys. Rev. A* **76**, 013607 (2007).
- [6] K. Bonin and V. Kresin, *Electric-Dipole Polarizabilities of Atoms, Molecules and Clusters* (World Scientific, 1997).
- [7] S. Deachapunya, A. Stefanov, M. Berninger, H. Ulbricht, E. Reiger, N. L. Doltsinis, M. Arndt, *J. Chem. Phys.* **126**, 164304 (2007).
- [8] B. Brezger, M. Arndt, and A. Zeilinger, *J. Opt. B* **5**, S82 (2003).
- [9] M. Arndt, K. Hornberger, and A. Zeilinger, *Physics World* **18**, 35 (2005).
- [10] M. K. Oberthaler, S. Bernet, E. M. Rasel, J. Schmiedmayer, and A. Zeilinger, *Phys. Rev. A* **54**, 3165 (1996).
- [11] R. Antoine, I. Compagnon, D. Rayane, M. Broyer, P. Dugourd, N. Sommerer, M. Rossignol, D. Pippen, F. C. Hagemeister, and M. F. Jarrold, *Anal. Chem.* **75**, 5512 (2003).
- [12] R. Antoine, I. Compagnon, D. Rayane, M. Broyer, P. Dugourd, G. Breaux, F. C. Hagemeister, D. Pippen, R. R. Hudgins, and M. F. Jarrold, *Eur. Phys. J. D* **20**, 583-587 (2002).
- [13] Y. Zhang, and E. Hannah, and T.-W. Koo, US patent, US 6,974,926 B2 (2005).
- [14] A. Hagen and T. Hertel, *Nano Lett.* **3**, 383 (2003).
- [15] D. A. Heller, R. M. Mayrhofer, S. Baik, Y. V. Grinkova, M. L. Usrey, and M. S. Strano, *J. Am. Chem. Soc.* **126**, 14567 (2004).
- [16] M. Marksteiner, G. Kiesewetter, L. Hackermüller, H. Ulbricht, M. Arndt, and A. Zeilinger, *Acta Phys. Hung. B* **26**, 87 - 94 (2006).
- [17] L. X. Benedict, S. G. Louie, and M. L. Cohen, *Phys. Rev. B* **52**, 8541 (1995).
- [18] W. D. Knight, K. Clemenger, W. A. de Heer, and W. A. Saunders, *Phys. Rev. B* **31**, 2539 (1985).
- [19] B. Kozinsky and N. Marzari, *Phys. Rev. Lett.* **96**, 166801 (2006).
- [20] W. A. de Heer, *Rev. Mod. Phys.* **65**, 611 (1993).
- [21] A. Mayer, *Appl. Phys. Lett.* **86**, 1 (2005).
- [22] H. B. G. Casimir and D. Polder, *Phys. Rev. B* **73**, 360 (1948).
- [23] O. Nairz, B. Brezger, M. Arndt, and A. Zeilinger, *Phys.*

- Rev. Lett. **87**, 160401 (2001).
- [24] S. Gerlich, L. Hackermüller, K. Hornberger, A. Stibor, H. Ulbricht, M. Gring, F. Goldfab, T. Savas, M. Múri, M. Mayor, and M. Arndt, Nature Physics, to be published (2007).